On the characterization of sandwich panels for solar flat plate collectors' applications: theoretical and experimental investigation

Djemai Hocine[1]✉, Hecini Mabrouk[2], Adnane Labed[2]

1 Laboratoire de Génie Energétique et Matériaux (LGEM), Université de Biskra, B.P. 145 R.P. 07000, Biskra, Algeria

2 Laboratoire de Génie Mécanique (LGM), Université de Biskra, B.P. 145 R.P. 07000, Biskra, Algeria

Received 19 April 2015
Revised 12 March 2016
Accepted 14 March 2016
Published online: 27 March 2016

Keywords
Sandwich panels
Flat plate collector
Thermal efficiency
Cork agglomerate
Polystyrene
Overall stiffness

Abstract: This paper presents an experimental characterization on the mechanical behaviour of four different sandwich panels, for use in thermal insulation. These Panels are the results of the combination of four composite materials; two materials as skins (Glass-Polyester and Plywood) and two as cores (Polystyrene and Cork agglomerate). From the comparison between the mechanical behaviour of these four sandwich panels which was tested for three point-bending tests; the sandwich with Glass-Polyester as skin and Cork agglomerate as core has the highest overall stiffness compared to the other sandwich panels. Furthermore, thermal characteristics of these four panels (insulation materials) were numerically used in a comparative study of thermal performances of solar flat plate collectors, FPCs. Thus, we have proceeded to the comparison of these FPCs efficiencies in order to determine the best performing model for agro-alimentary drying applications. From the comparison between these four FPCs, the highest efficiency was obtained from the FPC insulation panel with plywood as skin and cork agglomerate as core.

1. Introduction

We present in this study a light-weight material, with an excellent thermal insulation and high resistivity for solar Flat Plate Collectors' applications. Introducing sandwiches to these FPC showed very important improvements such as, low conductivity and strong insulation (Bailleul et al. 1996, Djemai et al. 2014). The insulation material is used in the bottom of collectors to reduce the loss of heat. It is composed of core panel sandwiched between two skin sheets. Composite sandwich structure is made of two thin-rigid face sheets and a light-thick core material (Abdi et al. 2014, Corigliano et al. 2000).

The absorber plate, the cover and the sandwich panels used in rear insulation are solicited by several constraints, such as the weight of collectors and wind constraints. For this reason, bending test is the most important proof in the study of mechanical behaviour of sandwich panels.

The best way to use solar energy for heating and drying is to convert it into thermal energy through solar collectors. Solar air and water heaters are FPCs which are generally used for heating air and water respectively. Solar air heaters are simple compact compared to solar water heaters (Duffie and Beckman 1991). In our laboratories, several theoretical and experimental investigations were carried out to estimate the enhancement of thermal performances of FPCs designed for drying (Aoues et al. 2009, Labed et al. 2011, 2015). In all these studies, the authors have used different forms of obstacles mounted under the absorber plate on the air channel duct.

In the present work, an experimental and numerical study was conducted to evaluate the mechanical behaviour and thermal performances of four FPCs with different composite materials insulation *"Polystyrene or Cork Agglomerate as a core and Glass-Polyester or Plywood as skins*".

These insulation materials (sandwich panels) are:

- W1: Polystyrene core between two external layers of Plywood;
- W2: Cork Agglomerate core between two external layers of Plywood;
- G1: Polystyrene core between two external layers of Composite material;
- G2: Cork Agglomerate core between two external layers of Composite material.

2. Materials and methods

2.1 Materials

The materials used for the production of the sandwich panels were:

✉ Corresponding author. E-mail address: djemaihocine45@yahoo.com

Fax: +213 33 543 148

Nomenclature

b	Width of the sandwich, mm
B	Width of the specimen in the test of the skin, mm
Cp_a	Specific heat of air, J $kg^{-1}K^{-1}$
D_b	Bending stiffness, N mm^2
D_G	Average values of overall stiffness, N mm^{-1}
D_o	Overall stiffness, N mm^{-1}
D_h	Hydraulic diameter, m
e	Height of the dynamic air vein in solar collector, m
E_{Sb}	Modulus of elasticity of the skin in the three point bending test, GPa
E_{st}	Modulus of elasticity of the skin in the tensile test, GPa
F_R	Heat removal factor of solar collector
F'	Efficiency factor of solar collector
F_o	Overall flexibility, mm N^{-1}
$h_{(abs-a)}$	Heat transfer coefficient between the absorber and the fluid , W m^{-2} K^{-1}
I_G	Global solar irradiance, W m^{-2}
P	Load, N
l	Length of the sandwich, mm
L	Length of the specimen in the test of the skin, mm
L_c	Length of the flat plate collector, FPC, m
l_c	Width of the FPC, m
$\dot{m}$	Air mass flow rate, kg s^{-1}
N	Number of cover
Nu	Nusselt number, non-dimensional number
Q_u	Useful energy gain of solar air collector, W
R	Thermal resistivity, m^2 K W^{-1}
Re	Reynolds number, non-dimensional number
S	Shear stiffness, N
S_{abs}	Collector surface area, m^2
S_a	Cross surface area in the dynamic air vein of collector defined in Eq. (14), m^2
t_c	Thickness of the core (insulation, mm
t_f	Thickness of the skin, mm
T_{amb}	Ambient temperature, K
T_{abs}	Mean absorber plate temperature, K
T_a	Mean fluid (air) temperature, °C
T_{ai}	Inlet air temperature of the collector, K
T_{ao}	Outlet fluid temperature of the collector, K
U_{ar}	Heat loss coefficient from the bottom of the back plate to ambient air, $Wm^{-2}K^{-1}$
U_{av}	Heat loss coefficient from the absorber plate to ambient air, $Wm^{-2}K^{-1}$
U_L	Global heat loss coefficient, $Wm^{-2}K^{-1}$
V_a	Average air velocity in the solar collector tunnel, ms^{-1}

Greek symbols

α_{abs}	Coefficient absorber
δ	Deflection, mm
ε	Strain, %
φ_g	Global incidence solar energy, W
φ_u	Useful energy gain of the solar collector, W
φ_l	Loss energy of the collector, W
φ_{st}	Stocked energy in the collector, W
λ_a	Thermal conductivity of fluid (air), $Wm^{-1}K^{-1}$
ν	Kinematic viscosity, m^2/s
σ	Stress, MPa
Δ	Difference

Subscripts

a	Air
ai	Air inlet
ao	Air outlet
o	Overall
f	Face
c	Core
sb	Bending test in the skin
st	Tensile test in the skin

- Cork agglomerates with 15 mm thickness to be used as core material in the sandwich panels;
- Polystyrene with 20 mm thickness to be used as core material in the sandwich panels;
- Plywood with 3.5 mm thickness, to be used as a skin in sandwich panels;
- Glass-Polyester with 3.5 mm thickness, to be used as a skin in sandwich panels.

The natural cork was harvested from the Jijel forests (Algeria) and was treated to the cork agglomerates at the industrial ''Taleza cork'' at Skikda, (Algeria). The granules of the natural cork were assembled with polyurethane resin to prepare the cork agglomerates. Its density is 280 kg/m^3 and a thermal conductivity (λ) is 0.0375W/m2 K^{-1} (Lakreb et al. 2015).

The Glass-Polyester is composed of unsaturated polyester resin NORSODYNE S-2010-V (Table 1) and glass fibre (Table 2).

Table 1. Unsaturated polyester resin properties NORSOYNE S2010.

Viscosity at 26°C	Density at 20°C	Tensile strength	Elongation	Removing volume
275 dPa	1.20 g cm^{-2}	54 MPa	1.5 %	7.1 %

Table 2. Glass fibres properties "(G) Type E (Mat 300, Mat 450)".

Length	Diameter	Elastic modulus	Elongation	Density
10-15 mm	14 μm	73 GPa	4.4-4.5 %	2.60-2.82 g/cm ²

This composite plate is prepared at FIPEXPLAST facility located in Chlef (Algeria) by contact molding method. This plate (Glass-Polyester) contains four layers at 33.33% fiber rate.

2.2. Panels production

Our study is based on four types of composite materials, as indicated in table 3 (figure 1).

Table 3. Unsaturated polyester resin properties "NORSOYNE S2010.

	Sandwich panels	Skins / thickness	Core/thickness
a	W1	Plywood / 3.5mm	Polystyrene /20mm
b	W2	Plywood / 3.5mm	Cork Agglomerate/ 15mm
c	G1	Glass-polyester /3.5mm	Polystyrene /20mm
d	G2	Glass-polyester /3.5mm	Cork Agglomerate/ 15mm

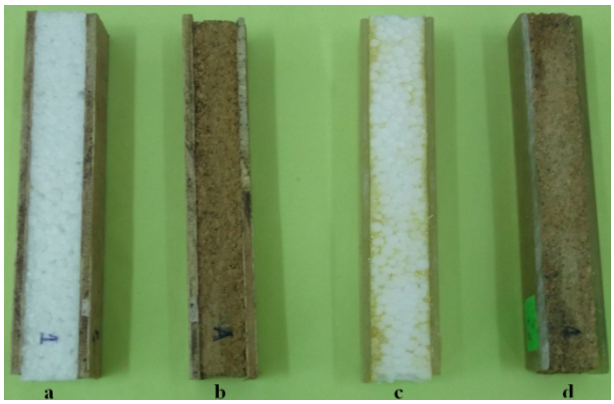

Fig. 1. Representation of sandwich panels assembly.

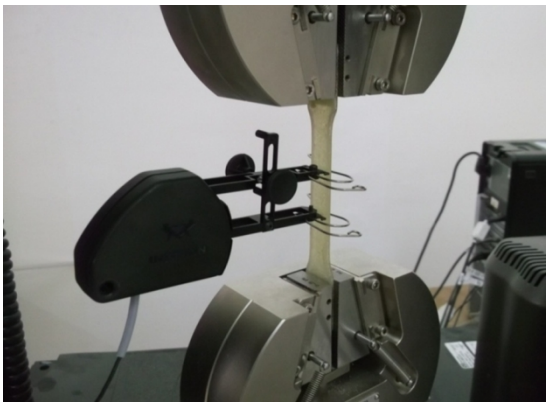

Fig. 2. Specimen between the jaws of machine with the extensometer.

2.3. Mechanical properties

Mechanical tests were performed with tensile and three point bending according to standards, respectively, (ASTM D638.2005, ASTM 790-81.2005, ASTM C393-62.1988). These tests were applied on skins only, and three point bending was applied on sandwich panels.

All these tests were conducted on "INSTRON" universal machine type 5969, with computer-controlled acquisition Bluehill3, with 5 and 50 kN force sensors, at the mechanical engineering department at the University of Biskra (Algeria).

2.3.1. Tensile tests on skins

Tensile tests were performed on specimens of 3.5 mm thickness, they are of the same skins material (Plywood and Glass-Polyester) (ASTM D638.2005) with a 50 kN force sensor and a constant crosshead speed of 2 mm / min, and placing extensometer (Fig 2) to determinate the real displacement on the specimen, and the mechanical properties were calculated from the stress-strain curves:

$$E_{st} = \frac{\Delta\sigma}{\Delta\varepsilon} \tag{1}$$

With E_{st} is the modulus of elasticity of skin and ($\Delta\sigma / \Delta\varepsilon$) is the slope in the stress-strain curve.

2.3.2. Three point bending tests on skins

Three-point bending tests were performed on 100x10 mm^2 specimen cut from skin (Plywood and Glass-Polyester) (NF EN ISO 178.2005).

This test was performed by applying load in perpendicular direction to the surface of specimen. This specimen was placed on two fixed supports within a distance of 60 mm from each other (Fig 3), using 5 kN force sensor and 2 mm/min constant crosshead speed. The mechanical characteristics were computed from the load-deflection curve.

For the analysis of a skin under three-point bending, consider a skin of width *B*, length L and thickness t_f (ASTM 790-81.2005):

$$E_{st} = \frac{\Delta P \times L^3}{\Delta f \times 4Bt_f{}^3} \tag{2}$$

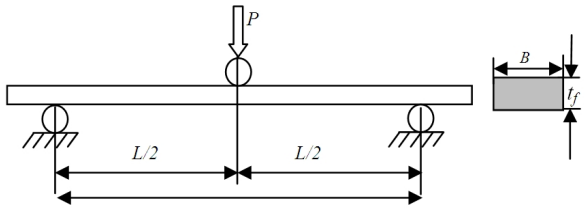

Fig.3. Sketch of skin under three- points bending showing geometrical parameters

With *(ΔP/Δf)* is the slope of the load-deflection curve.

2.3.3. Three point bending tests on sandwich panels

Three-point bending tests were performed on 140x20 mm^2 samples cut from the sandwich panels (W1, W2, G1 and G2) (ASTM C393-62.1988), Shahdin et al.2009). These tests were carried out by applying the load in the perpendicular direction to the surface of specimen. This specimen was placed on two fixed supports, within a distance of 80mm from each other (Fig.4), using 5 kN force sensor and 1mm min^{-1} constant crosshead speed. Mechanical characteristics were computed from the load-deflection curve. For the analysis of a sandwich beam under three-point bending test, consider a sandwich beam of width (b_s) and length (*l*), comprising two identical skins of thickness t_f and core of thickness t_c as shown in (Fig. 5). Elastic deflection expression can be expressed as (Shahdin et al. 2009):

$$\delta = \frac{Pl^3}{48D_b} + \frac{Pl}{4S} \tag{3}$$

$$\delta = \left[\frac{l^3}{48D_b} + \frac{l}{4S}\right]P \tag{4}$$

$$\delta = \left[F_0\right]P \tag{5}$$

$$P = \left[\frac{1}{F_o}\right]\delta \Rightarrow P = D_o\delta \tag{6}$$

With F_o is the overall flexibility of sandwich, and D_o is the overall stiffness of sandwich:

$$D_o = \frac{1}{F_o} \tag{7}$$

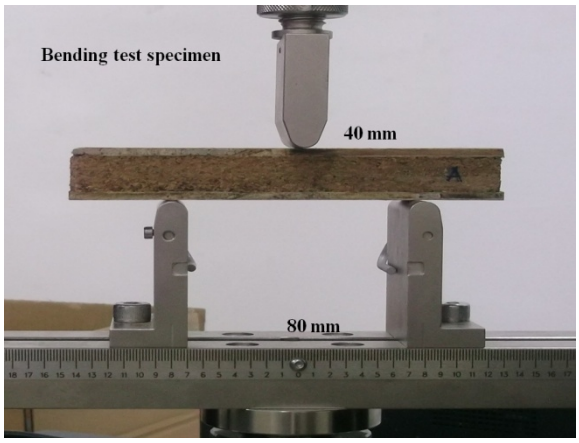

Fig. 4. Sandwich specimen between three supports during three- point bending test.

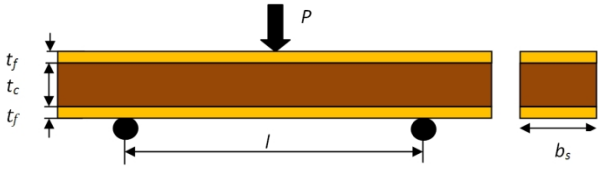

Fig. 5. Sketch of a sandwich beam under three-point bending showing geometrical parameters.

The overall stiffness of sandwich D_o is calculated experimentally by the three-point bending test, where D_o is slope of load deflection-curve.

The obtained equation (6) is only valid for the beginning of the bending tests when the deflection is relatively small.

3. Results and discussions

3.1. Tensile tests on skins

Figure 6 shows skins stress-strain curves (Glass-Polyester, Plywood) in tensile tests and Table 4 presents the average values of tensile properties of Plywood and Glass-Polyester materials. The behaviour under tensile test showed three areas: in the first area small linear increase of applied stress followed by weak linear stress up to the maximum value in second area, and finally stress decreased to rupture. Despite the second part is linear but it is not an elastic area because in this part there is a break on Polyester resin in the Glass-Polyester material and the interior falls in the Plywood. The tensile behaviour of the two types of skins was similar; although the stress was higher at rupture in Glass-Polyester material compared to Plywood. Glass-Polyester elasticity modulus is higher compared to Plywood elasticity modulus.

Table 4. Reports Average values of tensile properties, E_{st}, of Plywood and Glass-Polyester material.

Specimens	E_{st} (1) [GPa]	E_{st} (2) [GPa]	E_{st} (3) [GPa]	E_{st} (average) [GPa]
Plywood	2.744	2.204	2.765	2.568
Glass-Polyester	5.021	4.891	5.079	4.997

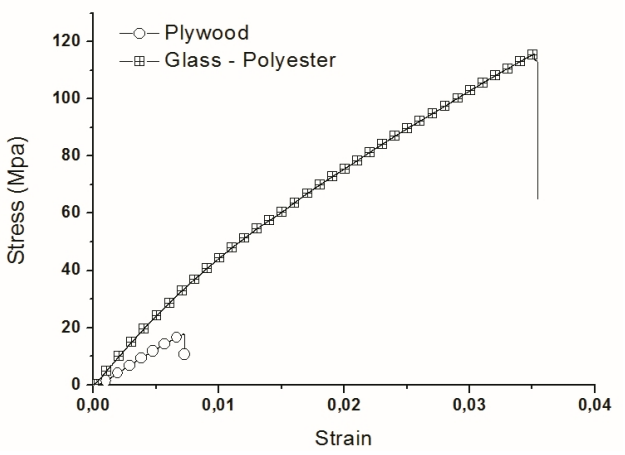

Fig. 6. Stress Strain curves for the skins (Glass-Polyester, Plywood) under tensile tests.

3.2. Three point bending tests on skins

Figure 7 shows Load-Displacement curves for skins (Glass-Polyester, Plywood) in three point bending tests. Table 5 presents the average values of elasticity modulus of Plywood and Glass-Polyester material. Load–Displacement curves under three point bending test showed three phases: A linear increase of the applied load at the beginning, then by a non- linear behaviour until the maximum load was reached, and finally a decrease of force to total rupture. The bending behaviour of both types of skins was similar; while a higher load at rupture in Glass-Polyester material compared to Plywood. Same as tensile test, elasticity modulus of Glass-Polyester in bending test is higher than in Plywood.

Table 5. Reports Average values of three point bending properties of plywood and Glass-Polyester material.

Specimens	E_{Sb}(1) [GPa]	E_{Sb}(1) [GPa]	E_{Sb}(1) [GPa]	E_{Sb}(average) [GPa]
Plywood	5.021	5.700	4.848	5.394
Glass-Polyester	7.177	7.721	7.468	7.455

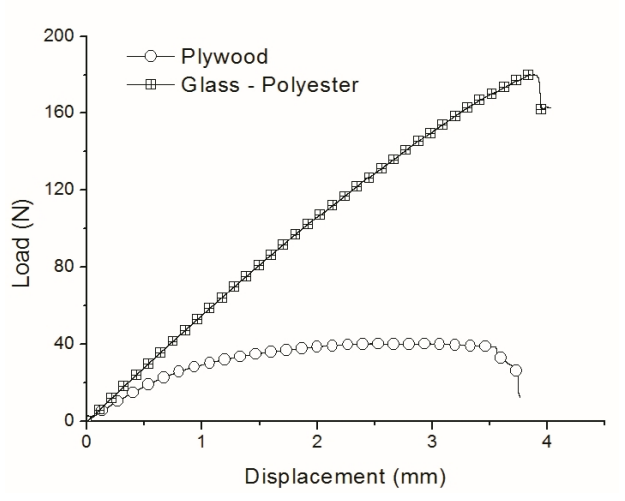

Fig. 7. Load displacement curves for skins (Glass-Polyester, Plywood) under three point bending tests.

3.3. Three point bending tests on sandwich panels

Figure8. Shows a typical load-deflection curve obtained under static three-point bending on four types of sandwich panels studied in this document (G1, G2, W1 and W2). Table 6 presents the average values of overall stiffness D_G (N mm^{-1}) which is obtained experimentally from load-deflection curve. The bending behaviour shows three parts: a first part corresponding to linear increase of load with arrow, then by second part of non-linear behaviour up to the maximum value of load, and a final decrease of load until sample failure. The bending behaviour of these four types of sandwich was similar; although the overall stiffness in (G2, W2) is higher compared to (G1, W1). Overall stiffness values are constant on each type of sandwich; it is dependent to the geometry and material (skins elasticity modulus and core shear modulus).

4. Thermal performances of FPCs with different composite insulation materials

4.1 Presentation of the proposed models

The considered system is "flat plate solar air heater", in its many forms; this kind of collector is by far the most common type of solar air heating collector. Its little maintenance and low cost have made it the choice in many domestic and commercial systems for solar air heating and drying.

In this study, four types of solar air heating collectors were numerically compared for their thermal performances. Therefore, the components of the collectors have the same size: thickness of the single cover glass (5 mm), height of the air gap between the cover and the absorber plat (25 mm), height of the air duct

Table 6. Overall stiffness D_G in deferent types of sandwich panels.

Sample	D_G (1) [N mm^{-1}]	D_G (2) [N mm^{-1}]	D_G (3) [N mm^{-1}]	D_G (average)	standard deviation
G1	26.03	25.70	26.17	25.97	0.24
G2	283.30	295.30	290.70	289.80	6.05
W1	36.59	31.90	32.46	33.60	2.59
W2	178.30	189.80	188.30	185,50	6.25

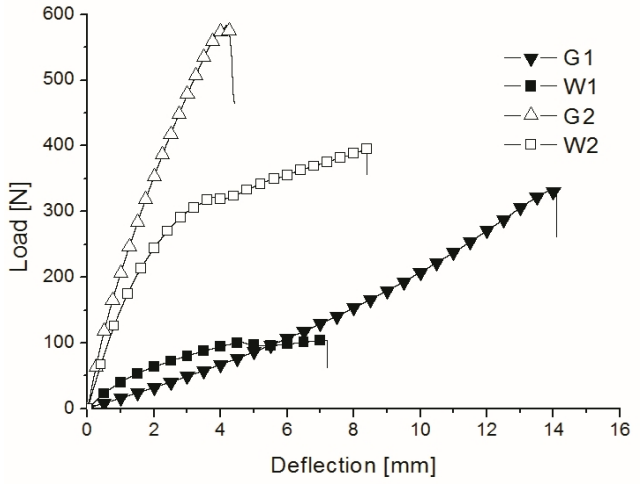

Fig. 8. Load–deflection curves for three points bending of the four types of sandwich panels.

(25 mm), dimensions of the absorber (1.96 m × 0.9 m with the thickness of 0.4 mm). Only the materials and thickness of the rear insulation are different.

The materials of the proposed FPCs components are the same (Fig. 9). The absorbers were made of galvanized steel with black non selective coating. The heated air flows between the inner surface of the absorber plate and the back plate.

In the first FPC model (W1), the rear and lateral insulation is provided by a polystyrene sheet (20 mm of thickness), which is sandwiched between two plywood sheets (t_f = 3.5 mm).

In the second FPC model (W2), the rear and lateral insulation is provided by a cork agglomerate sheet (20 mm) sandwiched between two plywood sheets (t_f = 3.5 mm).

In the third FPC model (G1); the rear and lateral insulation is provided by a polystyrene sheet (20 mm of thickness), sandwiched between two glass fiber sheets (t_f = 3.5 mm).

In the fourth FPC model (G2); the rear and lateral insulation is provided by a cork agglomerate sheet (t_c = 20 mm) sandwiched between two glass fiber sheets (t_f = 3.5 mm).

4.2. Theoretical analysis

Before the presentation of different configurations described above, we present the expressions used for the calculation of thermal resistivity, global heat loss, useful energy, and efficiency of the solar collectors.

Assuming one-dimensional heat flow considering thermal capacity and temperature drop across the rear insulation (Fig.10), the total thermal resistivity can be given

$$R = R_S + R_C + R_S = R_C + 2.R_S \quad (9)$$

Were $R = t / \lambda$

The method selected for modelling the performances of this collector is the global method which supposes that all the components of this section are at a constant average temperature. The numerical program used in this study was developed by (Aoues et al. 2009) for the calculation of the thermal performances of FPCs with different artificial roughness mounted in the dynamic air vein. The collectors operate under quasi steady-state conditions. The performance of the solar collector is described by an energy balance that indicates the distribution of incident solar energy into useful energy gain, energy stored, and energy losses.

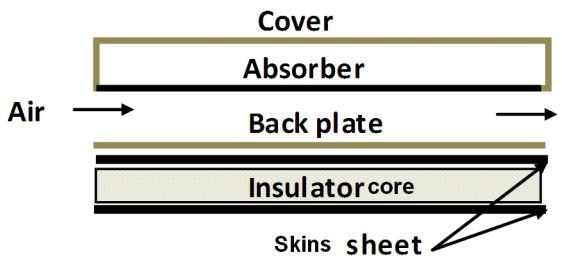

Fig. 9. Schematic view of FPC model.

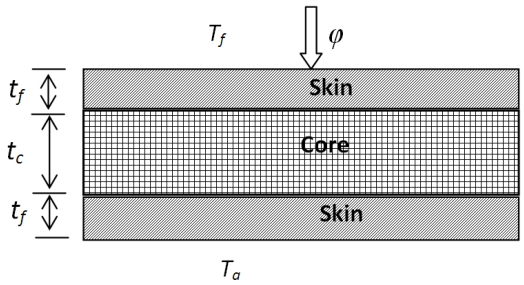

Fig. 10. Schematic view of the heat loss through the sandwich panel.

$$\phi_g = \phi_u + \phi_l + \phi_{st} \tag{10}$$

By neglecting the thermal energy stored (thermal inertia) in the collector, we obtain

$$\phi_g = \phi_u + \phi_l \tag{11}$$

The useful heat gain by a collector can be expressed as

$$\phi_u = \dot{m} \cdot Cp_a \cdot \left(T_{ao} - T_{ai}\right) \tag{12}$$

While introducing the collector overall loss coefficient between the absorber and the ambient air U_L, the useful energy gain provided by the collector (Duffie and Beckman 1991) as given by Eq. (16).

$$\phi_u = F_R\left[I_G\left(\tau_v\alpha_{abs}\right) - U_L\left(T_{ai} - T_{amb}\right)\right] \tag{13}$$

The heat removal factor, F_R is defined by Eqs. (14).

$$F_R = \frac{\dot{m} \cdot Cp}{S_{abs}U_L}\left[1 - \exp\left(-\frac{F' \cdot U_L \cdot S_{abs}}{\dot{m} \cdot Cp_a}\right)\right] \tag{14}$$

The collector efficiency factor F' and collector overall loss coefficient U_L for the studied configurations shown in Fig. 11, are obtained from the energy balances on the absorber plate, the fluid, and the back plate (Duffie and Beckman. 1991):

$$F' = \frac{h_{abs-a}\left(U_{ar} + 2h_{rabs-pl} + \cdot h_{abs-a}\right)}{\left(U_{av} + h_{rabs-pl} + h_{abs-a}\right)\left(U_{ar} + \cdot h_{abs-a} + h_{rabs-pl}\right) - h_{rabs-pl}^{\ 2}} \tag{15}$$

$$U_L = \frac{\left(U_{av} + U_{ar}\right)\left(h_{abs-a}^{\ 2} + 2.h_{abs-f}h_{rabs-pl}\right) + U_{ar}U_{av} \cdot h_{abs-a}}{h_{abs-a}U_{av} + 2.h_{abs-a}h_{rabs-pl} + h_{abs-a}^{\ 2}} \tag{16}$$

An empirical formula for the loss coefficient through the top of the collector U_t was developed following the basic method of (Hottel and Woertz 1942):

$$U_t = \left[\frac{N}{\frac{C}{T_{abs}}\left[\frac{\left(T_{abs} - T_{amb}\right)}{\left(N + f\right)}\right]^e} + \frac{1}{h_w}\right]^{-1} + \left[\frac{\sigma\left(T_{abs} + T_{amb}\right)\left(T_{abs}^2 + T_{amb}^2\right)}{\left(\varepsilon_{abs} + 0{,}00591 \cdot Nh_w\right)^{-1} + \frac{2N + f - 1 + 0.133\varepsilon_{abs}}{\varepsilon_v} - N}\right] \tag{17}$$

$$f = \left(1 + 0.089h_w - 0.1166h_w\varepsilon_{abs}\right)\left(1 + 0.07866N\right)$$

$$C = 520\left(1 - 0.000051\beta^2\right)$$

$$e = 0.430\left(\frac{1 - 100}{T_{abs}}\right)$$

T_{amb} is the ambient temperature (K), and T_{abs} is the mean absorber plate temperature (K).

For 70° < β < 90°, the loss coefficient through the bottom of the collector can be written:

$$U_{ar} = \frac{1}{\frac{t_C}{\lambda_C} + 2.\frac{t_S}{\lambda_S} + \frac{1}{h_{vv}}} \tag{18}$$

The outlet air temperature of the collector can be obtained from an energy balance (Duffie and Beckman 1991) as:

$$\frac{I_G \cdot \left(\tau_v\alpha_{abs}\right)_{eff} - U_L \cdot \left(T_{ao} - T_{amb}\right)}{I_G \cdot \left(\tau_v\alpha_{abs}\right)_{eff} - U_L \cdot \left(T_{ai} - T_{amb}\right)} = \exp\left(-\frac{S_{abs} \cdot F' \cdot U_L}{\dot{m} \cdot Cp_a}\right) \tag{19}$$

The mean temperatures of the absorber plate are obtained by solving the energy balance equations on these plates:

$$T_{abs} = 2T_a + \frac{Q_u}{h_{(abs-a)}} - T_{pl} \tag{20}$$

The instantaneous collector efficiency relates the useful energy to the total radiation incident on the collector surface by:

$$\eta = F_R\left(\tau_v\alpha_{abs}\right) - F_RU_L\frac{\left(T_{ai} - T_{amb}\right)}{I_G} \tag{21}$$

Here, $F_R\left(\tau_v\alpha_{abs}\right)$ and F_RU_L are two major parameters that constitute the simplest practical collector model. $F_R\left(\tau_v\alpha_{abs}\right)$ is an indication of how energy is absorbed and F_RU_L is an indication of how energy is lost. Besides, U_L is the collector overall heat loss coefficient.

The radiation heat transfer coefficient between the inner wall of the absorber plate and the galvanized sheet, where the temperatures T_{abs} and T_{pl} are expressed in Kelvin, written as (Sacadura 1980):

$$h_{r(abs-pl)} = \sigma\left(T_{abs} - T_{pl}\right)\left(T_{abs}^{\ 2} - T_{pl}^{\ 2}\right) / \left(\frac{1}{\varepsilon_{abs}} + \frac{1}{\varepsilon_{pl}} - 1\right) \tag{22}$$

In regard to the forced convection, the average heat transfer coefficient is given as

$$h_{(abs-a)} = h_{(pl-a)} = \frac{Nu\lambda_a}{D_h} \tag{23}$$

Where the Reynolds number is given by:

$$\mathrm{Re} = \left(V_a \cdot D_h\right) / \nu_a \tag{24}$$

The average velocity can be written as:

$$V_a = \frac{\dot{m}}{\rho_a \cdot S_a} \quad (27)$$

Where S_a and D_h are the dynamic air vein cross-surface area and the hydraulic diameter, respectively.

4.3. Theoretical results

4.3.1. Thermal Resistivity of different insulation materials

In recent years there have been an increasing number of applications such as communication, satellites, high density electronics, and advanced aircraft requiring more effective and light weight thermal management materials (Assael et al. 2008). The temperature fields in composites materials cannot be determined unless the thermal conductivity of the media is known and for any material a low thermal expansion is ideally required, which means a good thermal resistivity (Djemai et al. 2014 ; Devendra and Rangaswamy 2012 ; Kumlutas et al. 2003 ; Bozee et al. 2003).

In this part of the paper, we focused on the thermal performances that can be provided by different studied materials for different solar collectors and heat insulation applications.

Figure 11 shows the thermal resistivity of different studied composite materials as a function of their core thickness (t_f = 3.5 mm). It can be seen that the sandwich with cork agglomerate between two external sheets of plywood presents the best thermal resistivity, followed by the cork agglomerate sandwiched between two layers of glass polyester (when t_c > 14 mm), and the Polystyrene between two external layers of glass polyester presents the lower propriety.

The thermal resistivity of different composite materials as a function of the skin thickness t_f (t_c = 20 mm) are presented in fig. 12. It is clear that, for thickness values of the skin t_f less than 5 mm, the thermal resistivity of different materials remain in the same order; W2 followed by G2, than W1 and in the end G1, and Beyond t_c = 5mm the thermal resistivity of W1 becomes superior than that of G2.

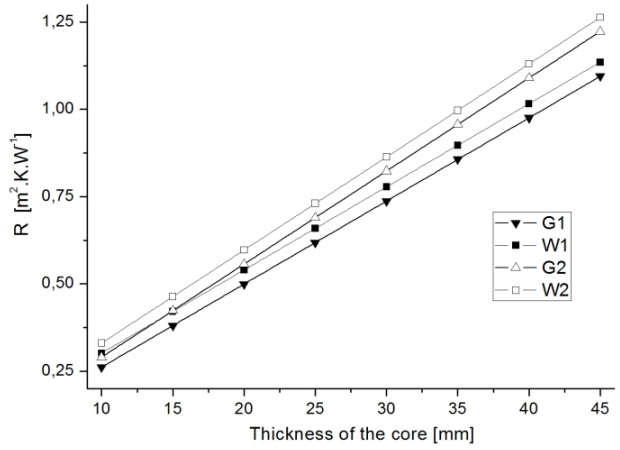

Fig.11. Thermal resistivity of different composite materials vs. the core thickness (the skin thickness = 3.5 mm.

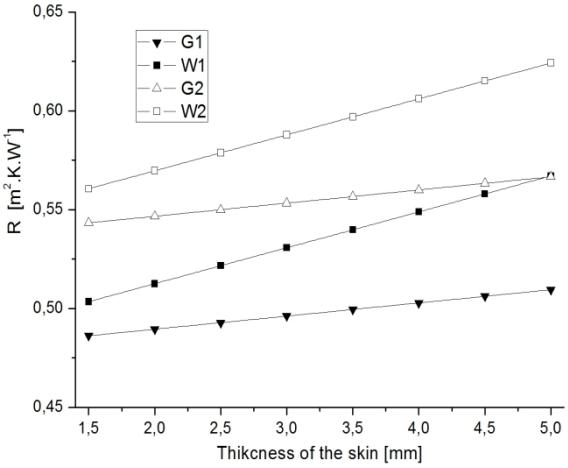

Fig.12. Thermal resistivity of different composite materials vs. the skin thickness (the core thickness=20mm).

4. 3.2 FPCs efficiencies

The theoretical results representing the performance of the solar collector are based on the Hottel, Whiller and Bliss approaches.

Fig. 13 shows the variation of the efficiency (η) of the FPC with different insulation materials as a function of the variation in the collector length. The improvements of thermal performances are important in relation to the FPC. The FPC with sheet of Cork agglomerates sandwiched between two external layers of Plywood (W2) presents the highest efficiency value 64% for a collector length of 2 m, while the FPC with layer of polystyrene sandwiched between two skins Glass-Polyester G1 presents the lowest efficiency 46% for the same collector length (2 m) and for the same flow rate (70 $m^3 h^{-1}$) (Figure. 13).

It is clear from Figure 14, that the highest outlet temperature is that produced by the FPC with sheet of Cork agglomerates sandwiched between two external layers of Plywood (W2 model), but the differences between the temperatures generated by both solar FPCs (W2 and G2) is not significant. In addition, the outlet temperature achieved by all FPCs with different composite materials can satisfy the energy needs for agro-alimentary drying applications (< 60°C).

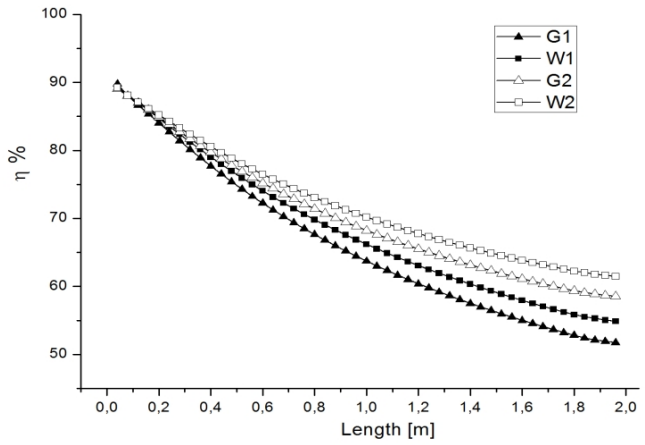

Fig.13. Efficiencies vs. FPC length (T_a = 25°C, T_{fe} = 27°C, I_G = 900 W m^{-2}, Q_v =70 $m^3 h^{-1}$).

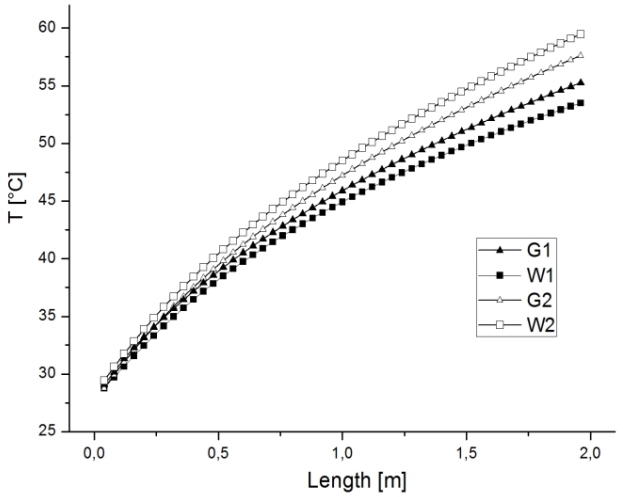

Fig. 14. Evolution of the exit temperature of FPCs with different insulation materials *vs*. the length of FPC.

5. Conclusion

An experimental investigation was provided, in order to characterize the mechanical behaviour of four sandwich panels for solar thermal applications.

From the comparison between the mechanical behaviours of both skins used in different types of sandwich panels, it is clear from the tests of tensile and the three points bending that, the elasticity modulus of the glass polyester sheet is higher than that of the plywood.

Through the experiments undertaken and according to the tests of three points bending it was found that, the overall stiffness of sandwich panel G2 is higher than the other sandwich panels (G1, W1 and W2).

However, a theoretical study was conducted to evaluate the thermal performances of four models of solar FPCs with different sandwich panels (W1, W2, G1 and G2) as insulation material. Thus, we have proceeded to the comparison of these FPCs in order to determine the best performing model for agro-alimentary drying application (T < 60°C).

From the comparison between these four FPC models with different composite insulation materials, the highest efficiency was obtained from the FPC with plywood and cork agglomerate sheet (W2 model). In addition, this study has allowed us to show that the outlet temperature achieved by the FPC with all these composite materials can satisfy the energy needs for agro-alimentary drying applications (< 60°C).

We could indicate here that, the humidity absorbance of G1 and G2 materials is lower than that of W1 and W2 materials, which is preferable for the agro-alimentary drying applications.

References

Abdi, B., S. Azwan, M. R. Abdullah, A. Ayob, Y. Yahia & L. Xin (2014) Flatwise compression and fexural behavior of foam core and polymer pin-reinforced foam core composite sandwich palnels. International journal of mechanical sciences. 88:138-144.

Aoues, K., N. Moummi., M. Zellouf., A. Moummi., A. Labed., E. Achouri. & A. Benchabane (2009) Amélioration des performances thermiques d'un capteur solaire plan à air: Etude expérimentale dans la région de Biskra", Revue des Energies Renouvelables 12(2): 237-248.

Assael, M. T., K. D. Antoniadis & D. Tzetzis (2008) The use of the transient hot-wires technique for measurement of the thermal conductivity of an epoxy-resin reinforced with glass fibers and/or corbon multiwall nanotubes. Composites science and technology 68(15-16): 3178-3183

ASTM (1988) Standard test method for flexural properties of flat sandwich constructions. C392-62.

ASTM (2005) Propriétés mécaniques des composites dans la pratique des essais. D 638.

ASTM (2005) Propriétés mécaniques des composites dans la pratique des essais. D 790-81.

Bailleul, J. L., G. Guyonvarch, B. Garnier, Y. Jarny & D. Delaunaya (1996) Identification des proprietés thermiques de composites fibres de verre / resines thermodurcissables ; Application à l'optimisation des procédés de moulage. Rev. Gén. Therm 35 : 65-77.

Bozee, Y., S. Kaang, P. J. Hine & I. M. Ward (2003) The thermal –expansion behavior of hot –compacted polypropylene and polyethylene composites. Composites science and technology. 60: 333-344.

Corigliano, A., E. Rizzi & E. Papa (2000) Experimental characterization and numerical simulations of a syntactic-foam / glass-fiber composite sandwich. Composites Science and Technologiy. 60: 2169-2180.

Devendra, K. & T. Rangaswamy (2012) Evaluation of thermal properties of E-Glass/Epoxy Composites filled by different filler materials. International Journal Of Computational Engineering Research. 2(5): 1708-1714.

Djemai, H., M. Hecini & A. Labed (2014) On the characterization of composite material for flat plat collectors. 7th International Conference on Thermal Engineering: Theory and Applications, Marrakesh, Morocco, May 06 - 08, 2014.

Duffie, J. A & W. A. Beckman (1991) Solar engineering of thermal processes: Second edition," New York, Wiley.

Hottel, H. & B. Woertz (1942) Performance of flat-plate solar-heat collectors.Trans. ASME, Am. Soc. Mech. Eng., United States 64: 91-104.

Kumlutaş, D., I. H. Tavman & M. Turhan Çoban (2003) Thermal conductivity of particle filled polyethylene composite materials. Composites science and technology: 63(1): 113-117.

Labed, A., N. Moummi, A. Benchabane, K. Aoues & A. Moummi (2011) Performance investigation of single- and double-pass solar air heaters through the use of various fin geometries. Int. J. of Sustainable Energy. 210: 423-434.

Labed, A., A. Rouag, A. Benchabane, N. Moummi & M. Zerouali (2015) Applicability of solar desiccant cooling systems in Algerian Sahara: Experimental investigation of flat plate collectors. Journal of Applied Engineering Science & Technology 1(2): 61-69.

Lakreb, N., B. Bezzazi & H. Pereira (2015) Mechanical behavior of multilayered sandwich panels of wood veneer and a core of cork agglomerates. Materials and Design. 65: 627–636.

NF EN (2005) Plastics determination of flexural properties amendment. ISO 178/A1.

Sacadura, J. F. (1980) Initiation aux transferts thermiques : Cast. INSA, Lyon, Paris.

Shahdin, A., L. Mezeix, C. Bouvet, J. Morlier & Y. Gourinat (2009) Fabrication and mechanical testing of glass fiber entangled sandwich beams: A comparison with honeycomb and foam sandwich beams. Composite Structures, 90(4), 404-412.